Proceedings of ASME Turbo Expo 2021
Turbomachinery Technical Conference and Exposition
GT2021
June 7-11, 2021, Virtual, Online

GT2021-58655

ASSESSMENT OF ENGINE OPERABILITY AND OVERALL PERFORMANCE FOR PARALLEL HYBRID ELECTRIC PROPULSION SYSTEMS FOR A SINGLE-AISLE AIRCRAFT

Sangkeun Kang, Ioannis Roumeliotis
Cranfield University, UK
Sangkeun.Kang@cranfield.ac.uk
i.roumeliotis@cranfield.ac.uk

Jinning Zhang, Vassilios Pachidis
Cranfield University, UK
Jinning.Zhang@cranfield.ac.uk v.pachidis@cranfield.ac.uk

Olivier Broca
Siemens Industry Software, France
olivier.broca@siemens.com

ABSTRACT

This paper aims to assess the gas turbine operability and overall hybrid electric propulsion system performance for a parallel configuration applied to a 150 passenger single-aisle aircraft. Two arrangements are considered: one where the low pressure shaft is boosted and one where the high pressure shaft is boosted. For identifying limits in the hybridization strategy steady state and transient operation are considered and the hybridization effect on compressor operability is determined.

Having established the electric power on-take limits with respect to gas turbine operation the systems performance at aircraft level is quantified for the relevant cases. Different power management strategies are applied for the two arrangements and for different power degrees of hybridization.

The results indicate that despite the fact that pollutant emission and fuel consumption may improved for hybrid propulsion, this comes at the cost of reduced payload and operability margins. Boosting the low pressure shaft may give the highest engine performance benefits but with a significant weight penalty, while the low pressure compressor system operability is negatively affected. On the other hand boosting the high pressure shaft provides lower engine performance benefits but with smaller weight penalty and with less operability concerns.

INTRODUCTION

Despite of COVID-19 crisis, modern aviation industry is considered the fastest-growing source of greenhouse gas emission, as annual air traffic is doubled in every 15 years for past decades [1]. ICAO proposed carbon neutral growth from 2020 onwards regardless of the increase in annual air traffic [2], while Europe through FlightPath2050 [3] aims for 75% reduction in CO_2 and 90% reduction in NO_x emissions per passenger km compared to 2000 values.

Hybrid Electric Propulsion System (HEPS) concept is considered a promising candidate for helping towards achieving these target [4]. Besides of CO_2 emission, a significant reduction in noise emission and high efficiency of electrical power train are possible advantages that can be claimed from electrification [5].

However, the low energy and power density of electric components is recognized as a major drawback [6]. The energy density of current technology electric batteries is about 45 times lower than that of kerosene [5], while more than 10 years of time is expected for reaching MW class EPS (Electric Propulsion Systems) as discussed in [7]. The introduction of Cryogenic technology and High-Temperature Superconducting (HTS) is considered as promising facilitator in the progress of electrical technologies for HEPS concept realisation ([8], [9]). The battery recharging or replacement time would be another aspect that have to be considered for HEP application, as the fastest charge rate up to date is around 450kW/h with prototype combined charging system charger [10].

Moreover, adequate thermal management system shall be provided in HEPS to maintain the ideal operating temperature for electrical system components [11]. Microchannel heat sinks, heat pipe, phase change materials and jet impingement method are promising thermal management techniques that can be applied for HEPS. A detailed discussion on these methods is provided by McCluskey et al. [12].

Lastly, operability and control issues are expected for HEPS arrangements, due to distinctly different system behaviour of the EPS against the conventional Gas Turbine. Particularly for parallel hybrid configurations, one or both power trains may provide the required propulsion power at any given time, hence, control technology requirements will be complicated as the reaction time of each propulsion system should be considered as discussed by Simon et al. [13]. Additionally, gas turbine

component matching is expected to be affected by the electrical drive and the power on-take [14].

This paper aims to assess the gas turbine operability and overall performance for a parallel hybrid electric turbofan propulsion system applied to a 150 passenger single-aisle aircraft. Two different HEPS arrangements are assessed since the electric power on-take can be used to boost either the low pressure (LP) shaft (Mechanically Integrated Parallel Hybrid - MIPH) or the high pressure (HP) shaft (Cycle-Integrated Parallel Hybrid-CIPH) [8]. Low pressure shaft power on-take has been assessed in several studies (e.g. [14], [15]), while high pressure shaft power on-take has not been investigated. The arrangements are assessed in terms of operability (steady state and transient) and in terms of performance, building on existing knowledge ([14], [15]) and expanding to the CIPH arrangement. The results indicate that operability may be a limiting factor when high degrees of hybridization are considered, while CIPH arrangement has some advantages in terms of operability and weight, which are worth investigating.

METHODOLOGY

An integrated propulsion system model has been developed for assessing the parallel hybrid electric turbofan performance and operability. The integrated model, developed in Simcenter Amesim, includes the aircraft model which provides the thrust requirements, the propulsion system model (conventional and hybrid) and correlations for NOx calculations. Additionally, a tool for electric components sizing has been developed for quantifying the added system weight for hybrid cases. Models for the following propulsion system arrangements are developed:

- CIPH arrangement where the electrical power train provides power to the HP shaft
- MIPH arrangement where the electrical power train provides power to the LP shaft

The integrated model schematic for the MIPH configuration is depicted in Figure 1. In this section the models and tools used in this work are discussed.

Aircraft Model

NASA FLOPS software [16] is used for aircraft sizing and for providing the thrust requirements for specific mission to the propulsion system model. The airframe model is based on the A320 aircraft geometry and features as provided by Lammen and Vankan [17] and Hoogreef et al. [18]. The model simulates the flight performance of the aircraft, at each operating point of the flight envelope, using a pseudo-3D approach.

Propulsion System

Two propulsion systems are considered herein, the conventional year 2000 turbofan that acts as the baseline and a parallel hybrid electric version of the baseline utilizing two different shaft power on-take arrangements (CIPH and MIPH). Three models have been developed in Simcenter Amesim system simulation platform utilizing the gas turbine library [19] and the electric component libraries ([20], [21]). The MIPH arrangement model is depicted in Figure 1. The fuel flow acts as the gas turbine setting parameter for matching the thrust requirement.

Electric Power Train

The electric power train consists of electric machine, converter, and battery pack. For the motor a fully superconducting electric machine is sized since it is considered as enabling technology for reducing the weight penalty. The sizing methodology proposed in [22] for a fully superconducting electric machine is used utilizing the data provided in Table 1. The methodology is based on torque per unit of rotor volume (TRV):

$$TRV = \frac{T}{V_m} = \frac{\pi}{\sqrt{2}} \cdot k_{\omega 1} \cdot A \cdot B \qquad (1)$$

Where $k_{\omega 1}$ is winding factor, A is electrical loading and B is average flux density. Through eq. (1) the volume V_m is calculated and then it is used in conjunction with aspect ratio (L_a/D_m) to calculate the mean stator winding diameter (D_m):

$$V_m = \frac{\pi}{4} D_m^2 L_a = \frac{\pi}{4} D_m^3 \left(\frac{L_a}{D_m}\right) \qquad (2)$$

Having established D_m, the outer stator radius is calculated through eq. (3), using mean stator factor (m).

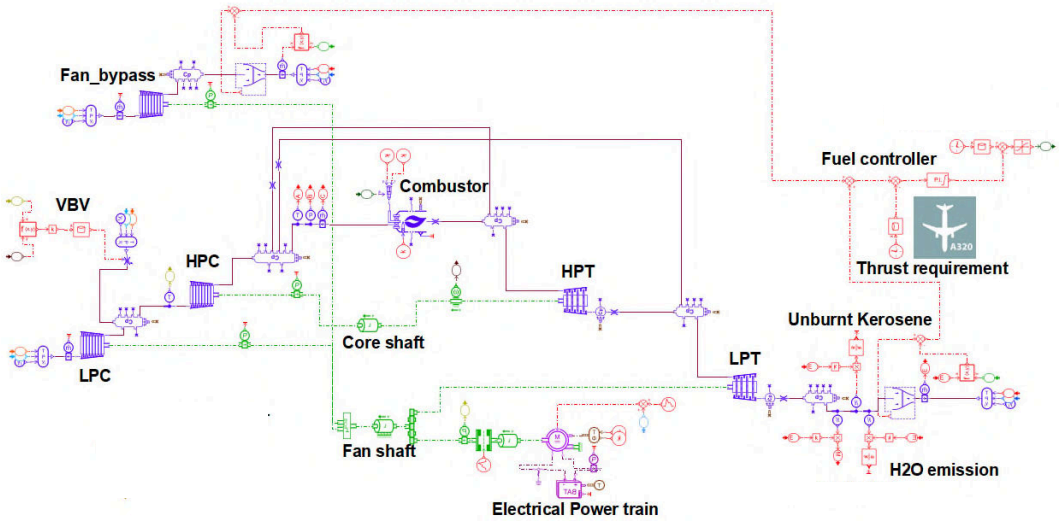

Figure 1 Parallel hybrid electric turbofan configuration

$$R_s = \frac{\left(\frac{a \cdot R_m}{1-m}\right) + b}{1 + \frac{m \cdot a}{1-m}} \quad (3)$$

Where a represents rotor and stator linear factor, and b represents rotor and stator adding factor which are fitted based on a survey on interior-rotor electric machines [22]. Then the total weight (W) is estimated as follows:

$$W = \frac{\pi}{4}(2 \cdot R_s)^2 \cdot L_a \cdot \rho(1 + wf) \quad (4)$$

Where L_a is active length calculated through D_m and aspect ratio, ρ is electric machine active density, a technology parameter, and wf is cryostat weight factor. The active power density is the main parameter affecting the motor weight and values in the range of 2000 to 8000 kg/m^3 are reported in [22], depending on the time horizon considered.

Table 1: Parameters for HTS electric machine sizing [22]

Parameter	Value
Winding factor $k_{\omega 1}$	0.9
Electrical loading A	80 kA/m
Average flux density B	1.8 T
Mean stator factor m	0.66
Cryostat adding weight factor wf	0.15
Aspect ratio L_a/D_m	1.8
Rotor/stator linear factor a	1.144
Rotor/stator adding factor b	83.03

The motor is simulated using the Simcenter Amesim functional electric drive and torque control model. The motor representation is done through a map that is scaled for each configuration examined herein. Specifically, the maximum torque, maximum power and maximum speed along with the torque and speed at maximum efficiency are used as scaling parameters (Figure 2). The design point efficiency is assumed 0.95 as suggested in [23] for all configuration.

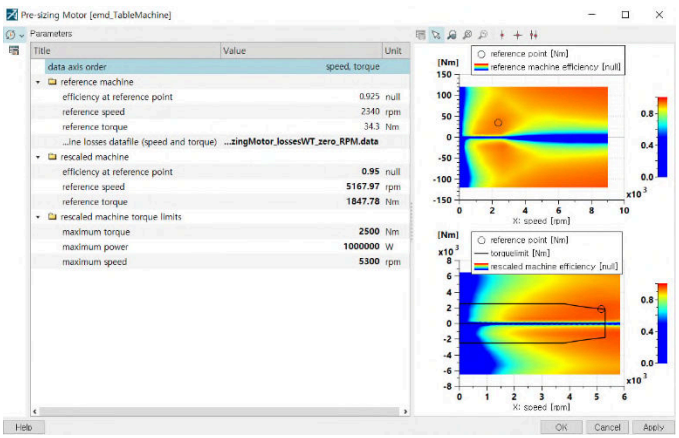

Figure 2 Pre-sizing motor function interface

The battery sizing algorithm is adapted from [24] and depicted in Figure 3. Battery nominal cell power (P_N), voltage (V_N) and capacity (Q_N), current load operating profile (i), charge reserve (q_L), non-load constant voltage (E_0) and internal resistance (R) are the main inputs, along with the voltage drop over the exponential zone (A) and the time constant of the exponential zone (B).

The number of parallel cells ($N_{parallel}$) is determined by total discharged capacity, calculated as the integral of current load profile for the discharge cycle and the battery cell nominal capacity considering the charge reserve. Then the operating current and discharge capacity at peak power load ($i_{batt,P}$ and $Q_{dis,batt,P}$ respectively) are calculated for establishing depleted energy (E_P) and estimating battery cell voltage output at peak power ($V_{batt,P}$). Finally, the cell peak load is calculated ($P_{batt,P}$) and used for establishing the number of battery cells (N_{cells}). Having established the battery cells, the battery weight is calculated via eq. (5) for specific battery energy density (ρ_{energy}).

$$W = \frac{N_{cells} \cdot V_N \cdot Q_N}{\rho_{energy}} \quad (5)$$

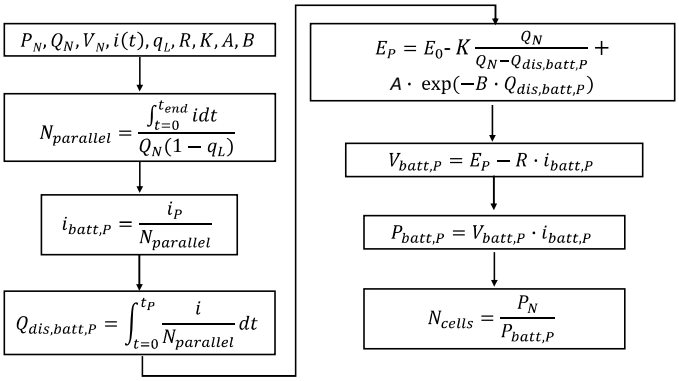

Figure 3: Battery sizing workflow adapted from [24]

The sizing battery cell parameters used in this study are listed in Table 2, adopted from [24]. The battery energy density ρ_{energy} is a critical parameter and future values reported in [25] are in the range of 400 to 2000 Wh/kg on cell level, depending on type, time horizon and assumptions.

Table 2: Cell data for battery sizing algorithm [24]

Input	Value
Nominal Power P_N	7.8 W
Nominal Voltage	1.2 V
Capacity V_N	6.8 Ah
Charge Reserves Q_N	20%
Constant voltage of battery under no load condition E_0	1.2848 V
Internal resistance of battery R	0.0046 Ω
Polarization voltage K	0.01875 V
Exponentiel zone drop voltage A	0.144 V
Exponential zone time constant inverse B	2.3077Ah^{-1}

The battery is simulated using the equivalent circuit model for battery pack available in Simcenter Amesim [26]. The model utilizes for each type of battery specific data sets of performance parameters (e.g. charge resistance) against charge reserve and temperature which are scaled based on the battery design data. It is capable to reproduce the battery performance and heat released during discharging as discussed in [27].

Gas Turbine

The powerplant is based on a conventional year 2000 turbofan with thrust requirements suitable for an A320-size aircraft (Table 3). The baseline powerplant (no-hybridisation) is able to deliver the T/O thrust without any electrical power on-take. The thermodynamic cycle design for the powerplant was performed using the Simcenter Amesim gas turbine performance tool. For off-design operation suitable maps, available in the Simcenter Amesim library are used, such as the HPC map depicted in Figure 4, along with the representative operating points for the baseline engine. For establishing low thrust simulation capability component maps were extended to low rotational speeds using the extrapolation method proposed by Gaudet and Gauthier [28]. A BOV is also applied to the model for ensuring low thrust operation utilizing a schedule based on CFM56-3 engine data published in [29]. The BOV is modelled as a controlled orifice with opening relative to the HP corrected rotational speed. The bleed-off during idle is 40% of core mass flow.

Table 3 Operating point performance parameter of Baseline engine

Operating point	Idle	Take-off	TOC	Cruise
Mach Nr (-)	0	0.25	0.78	0.78
Altitude (m)	0	0	10668	10668
WF (kg/s)	0.112	1.316	0.556	0.384
OPR (-)	4.38	27.51	33.32	27.64
Thrust (kN)	5.1	96.9	31	23.3
W_{BP} (kg/s)	61.3	285.9	114.5	108.5
W_{CORE} (kg/s)	18.9	58.3	24.5	22.0
TET (K)	888	1642	1585	1342
NHP (rpm)	10863	15745	14918	14088
NLP (rpm)	2180	5106	5062	4577

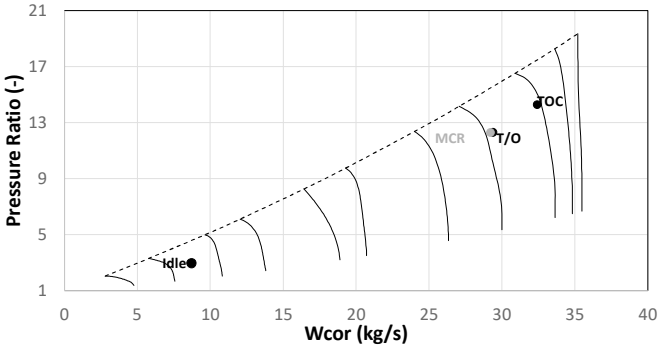

Figure 4: HPC representative operating points

The moment of inertia plays an essential role in the engine transient operation, which is expected to affect the HEPS operability. Cranfield University in-house software ATLAS ([30], [31], [32]) is used to estimate the LP and HP shaft moments of inertia (including turbomachinery components) based on engine performance data. The LP shaft moment of inertia is evaluated to 114.3 kgm^2 and the HP shaft moment of inertia is evaluated to 12.0 kgm^2. These values are used as input to the dynamic model for simulating transient operation.

The gas turbine CO_2 emissions are directly calculated by the model. NOx emissions are calculated by applying the P3T3 method [33]:

$$EINOx_{ALT} = EINOx_{GL}\left(\frac{P31_{ALT}}{P31_{GL}}\right)^{n} \cdot \left(\frac{FAR_{ALT}}{FAR_{GL}}\right)^{m} \cdot exp\left(19 \cdot (SH_{GL} - SH_{ALT})\right) \quad (6)$$

The ground level EINOx data used is the one reported in the ICAO emission databank [34] for an engine of similar thrust, namely CFM56-5B4/P. The ground level engine performance data used in the equation is derived by the model, since no engine data is available in the open literature (Table 4). The ground level engine parameters are correlated versus T31 and then corrected for altitude via eq. (6) using the altitude performance data calculated by the model. The exponent values are defined according to [33], namely n=0.4 and m=0, while specific humidity (SH) is calculated by the model according to ambient conditions.

Table 4 Ground Level Engine parameters

ICAO point	$T31_{GL}$ (K)	$P31_{GL}$ (barA)	FAR_{GL} (kg/kg)	$EINOx_{GL}$ (g/kg)
Idle	476.8	3.8	0.0135	4.3
Approach	619.0	10.8	0.0159	10
Climb out	759.3	24.8	0.0236	23.2
Take-off	795.2	28.5	0.0263	28

GAS TURBINE ASSESSMENT

Both Mechanically Integrated Parallel Hybrid (MIPH) and Cycle-Integrated Parallel Hybrid (CIPH) arrangements are simulated at representative steady-state operating conditions: Take-off (T/O), Top of Climb (ToC) and Cruise (MCR), to assess aspects of the engine performance and operability. Then, the operability of both configurations is assessed for rapid acceleration considering the different time constants of the two sub-systems (thermal engine and electric power train). The shaft power on-take is varied from 0.5 to a maximum of 2 MW for each case and operating point. The power degree of hybridization (DoH) is considered in this study:

$$DoH = \frac{P_{EL}}{P_{EL} + P_{GT}} \quad (7)$$

Steady State Operation

Electric power on-take for specific thrust requirements will reduce the fuel flow and the TET compared to the baseline (conventional) engine. This will be beneficial for emissions and engine life. The TET reduction is significant when T/O is considered, as seen in Figure 5 and can reach a value of 55 deg for power on-take equal to 2 MW (DoH 4%). The T/O TET reduction is similar for MIPH and CIPH arrangements, hence the relevant benefits in terms of life are expected to be similar. The fuel flow reduction is more profound when the low pressure shaft is driven by the electric system, as seen in Figure 6 and

this behaviour is consistent for climb and cruise as well, hence MIPH arrangement is expected to have higher performance benefits, in terms of block fuel. This performance behaviour is due to components re-matching that affects both cooling flows and components efficiency.

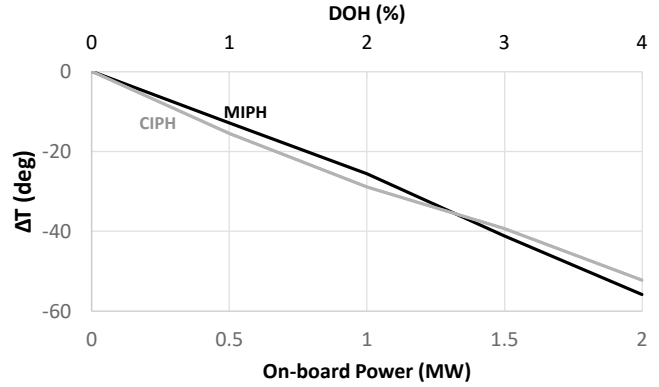

Figure 5: T/O TET reduction for different DoH

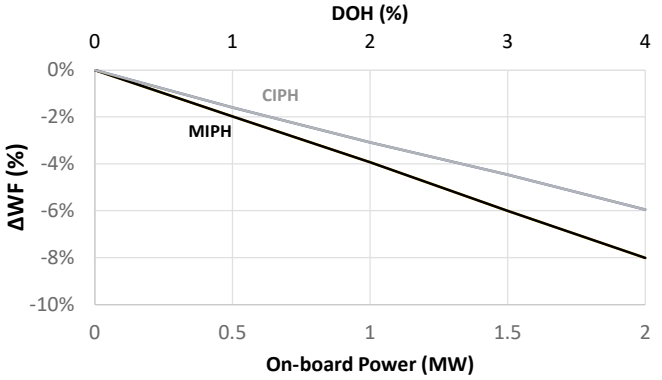

Figure 6: T/O fuel flow reduction for different DoH

As seen in Figure 7 components re-matching affects the pressure build-up and the core and by-pass mass flow rate. Specifically, core mass flow and OPR increases for the CIPH and decrease for the MIPH arrangement. This behaviour is expected, since for nominal operating points the HPT operating point is frozen given that the LPT is chocked. In this case $W_{HPTcor} = constant = \frac{Wcore \cdot \sqrt{TET}}{OPR}$, thus an increase in W_{CORE} results to an increase of OPR (CIPH) and the opposite occurs when W_{CORE} decreases.

The change of OPR and pressure distribution affects the secondary air system boundary conditions, changing the turbine cooling flows. The cooling flow reduces by approximately 5% for the MIPH arrangement and for power on-take of 2MW, reducing the potential TET benefit and providing higher fuel benefit compared to the CIPH. The better performance of the MIPH configuration is further justified by observing the LPC operating point. As seen in Figure 9 the LPC operation for CIPH arrangement is close to the choke region which is typically a low efficiency region. For the 1 MW power on-take case the LPC efficiency is 0.885 for MIPH and 0.856 for CIPH arrangement and for the maps used herein.

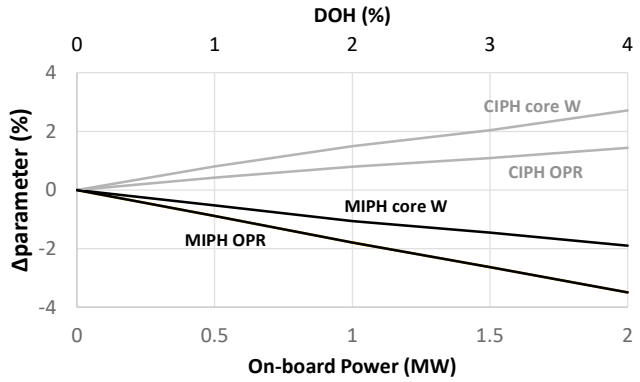

Figure 7: T/O OPR and core mass flow for different DoH

Additionally, hybridization may affect the gas turbine engine operability. Electrically driving the LP shaft will reduce the LPC surge margin as depicted in Figure 9 and reported by Sahoo et al. [14] and Wortmanm et al. [15]. Electrically driving the HP shaft (CIPH arrangement) moves the LPC operating point towards choke. In both cases DoH limit should be considered for avoiding potential fluttering (stall or choke). This limiting behaviour will be more important during engine transient operation. For the CIPH arrangement the HPC operates at higher rotational speed (Figure 10), a change that may affect the ToC operation and the system mechanical integrity. Concerning the fan, as seen in Figure 8 its operation is not significantly affected for the power on-take considered herein.

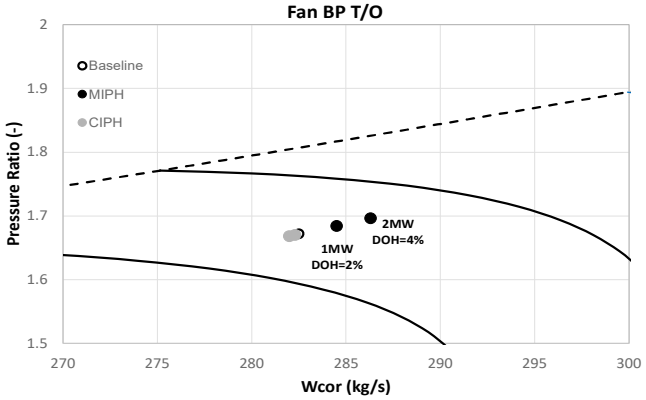

Figure 8: T/O Fan BP operating points for different DoH

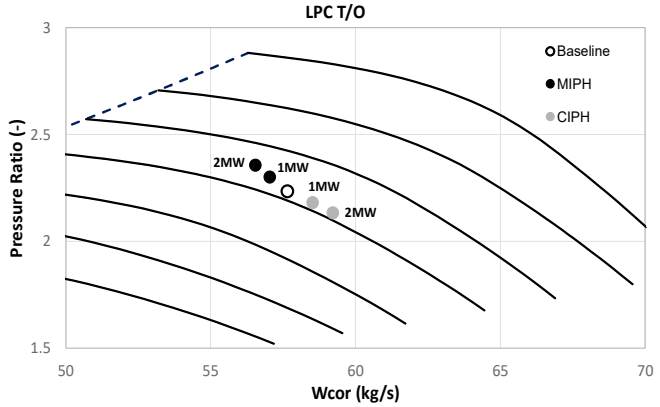

Figure 9: T/O LPC operating points for different DoH

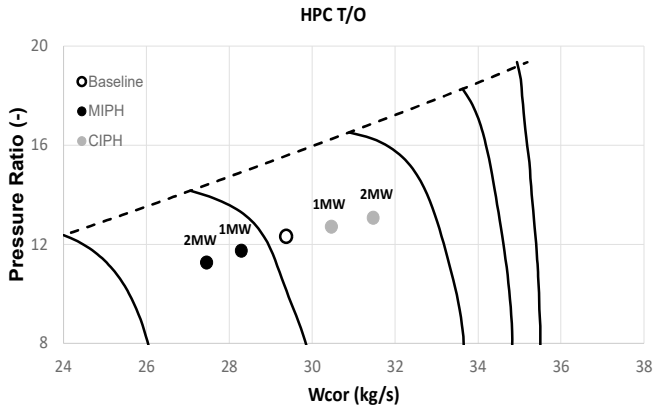

Figure 10: T/O HPC operating points for different DoH

For ToC, applying DoH higher than 5% (approx. 1 MW) significantly increases the fan rotational speed for the LP drive arrangement (MIPH) and the HP rotational speed for the HP drive arrangement (CIPH), as seen in Figure 11 and Figure 13 hence a limit on DoH should be imposed for ensuring mechanical integrity. The LPC behaviour is similar with the T/O case, where operating points move towards stall for the MIPH arrangement and towards choke for CIPH arrangement.

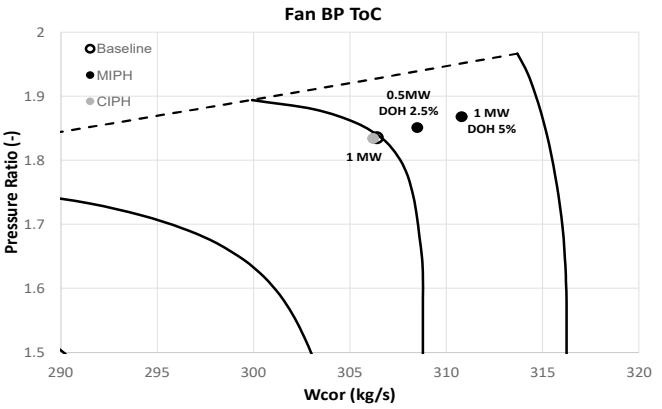

Figure 11: ToC Fan BP operating points for different DoH

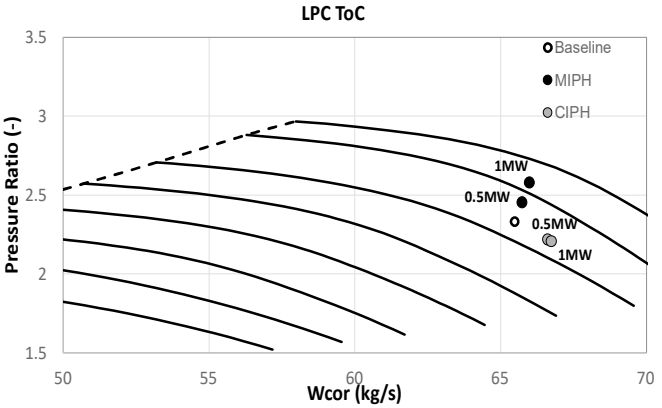

Figure 12: ToC LPC operating points for different DoH

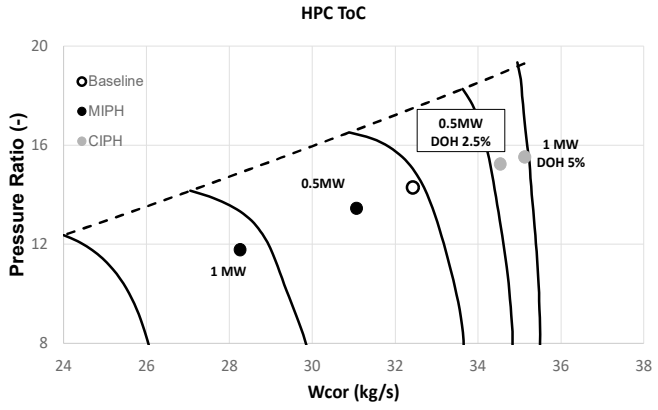

Figure 13: ToC HPC operating points for different DoH

Concerning MCR, the DoH that can be used is higher compared to the ToC one, as seen in Figure 14. The engine can accommodate 1.3 MW of power on-take (DOH=8%) and still have significant surge margin, while there is no HPC over-speeding for DoH up to 12% (2MW).

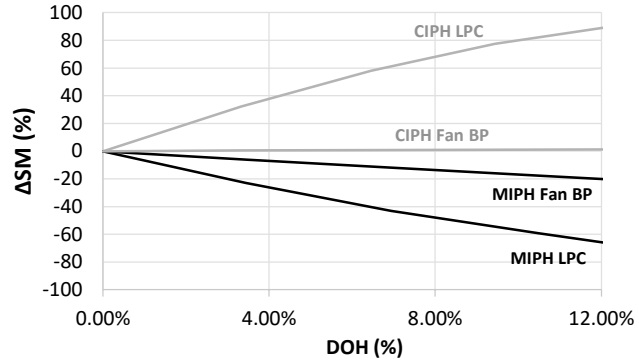

Figure 14: MCR Surge Margin change for different DoH

Transient Operation

A reference sea level acceleration profile, from idle to ICAO T/O (120kN in this case) depicted in Figure 15 is used for assessing the operability of the engine. For the HEP cases fuel flow adapts for accommodating the power on-take.

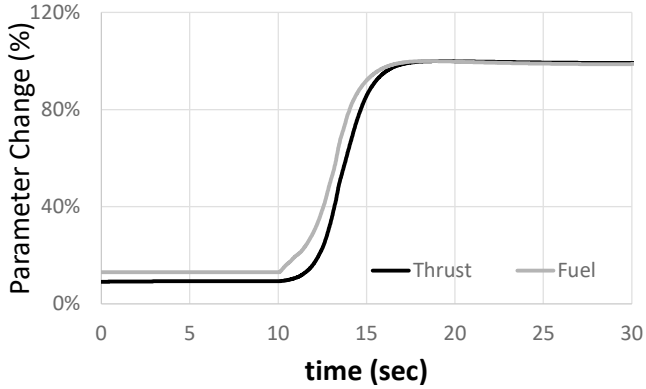

Figure 15 Reference slam acceleration profile

As seen in Figure 16 the HPC surge margin during acceleration is not negatively affected by the values of DoH simulated herein. It is interesting to note that directly driving

the HP shaft (CIPH) decreases the transients of the HPC and its acceleration operating line resembles the steady state operating line. The acceleration operating line for the MIPH arrangement follows the baseline engine operating line in terms of surge margin. The fan BP acceleration line is practically unchanged for both hybrid electric arrangements and follows the baseline engine operating line, due to the shaft high inertia.

For the LPC, the steady state assessment highlighted that the MIPH arrangement may have stability issues. This is confirmed for the acceleration case examine herein. As seen in Figure 17 the surge margin rapidly reduces to 0% for the MIPH arrangement. An interesting observation is that the BOV utilized is not working as designed. Specifically, for the CIPH case the HP shaft acceleration is faster than expected, hence the BOV starts closing prematurely, while the opposite occurs for the MIPH arrangement. In this context it is essential to rethink the engine stability control as we move towards hybridization and what parameters should be considered. Additionally, the CIPH arrangement may have an advantage during part load since the bleed off mass flow (BOV opening) can decrease offering a potential benefit in phases such as descent.

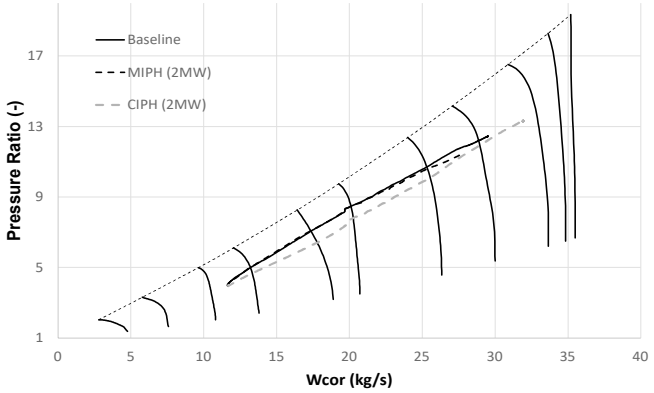

Figure 16 HPC operating line during slam acceleration

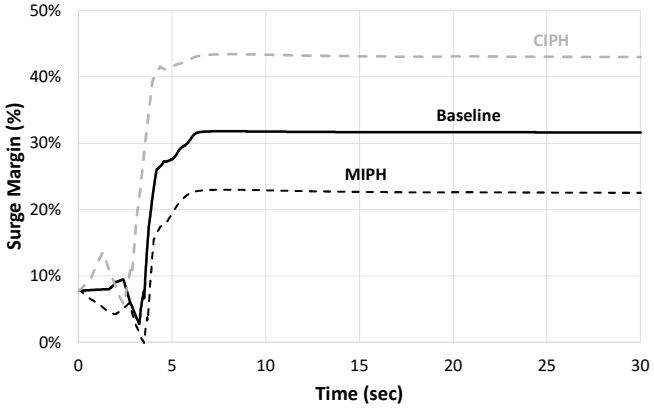

Figure 17 LPC surge margin change during slam acceleration

SYSTEM PERFORMANCE ASSESSMENT

For assessing the performance of the CIPH and MIPH arrangements 5 different Power Management Strategies (PMS) are considered. T/O and partial climb (T/O & P CL) is designed to assess the hybridisation effects for a short duration and aims to reduce T/O TET and emissions close to the airport. The electric power plant provides power (1 or 2 MW, depending on the case) up to 10000 ft altitude. T/O and climb strategy (TO & CL) utilizes the electric power train up to 30000 ft. The power on-take is bounded to 1 MW to avoid operability issues at ToC.

Descent is a flight phase that may be benefited by hybridization, since the engine operates at low power setting and at high sfc. Hybridization for whole and for part of the descent phase is examined herein (DSCNT and P DSCNT respectively). Additionally, the case of one engine fully electric descent (FE DSCNT) is considered. In this case one engine is driven by electric power with a maximum shaft power on-take of 3.3MW, while the second engine operates only on fuel. It should be highlighted that for these cases the BOV schedule and opening is kept the same as that of the baseline engine.

Two missions are used for assessing the HEPS performance, 1000 nmi and 2500 nmi. The 1000 nmi mission and the phases where electric boosting is applied are depicted in Figure 18**.**

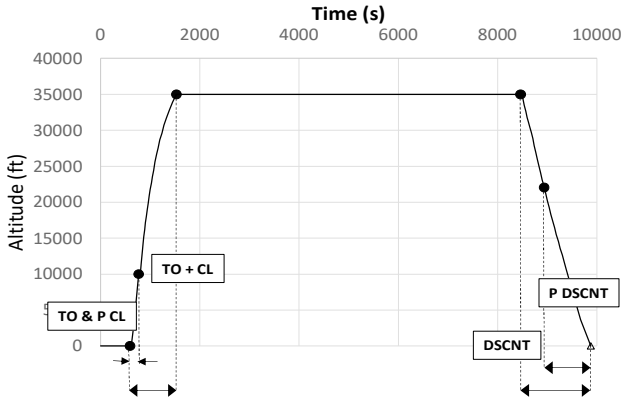

Figure 18: Mission density altitude and PMS

Electric Components Sizing

For each power management strategy, the electric power train is resized based on power and energy requirements and shaft rotational speed. The battery energy density is set to 1000Wh/kg [25], following the 20 years projection suggested in [35] and the motor active density is set to 8000kg/m^3 ([22], [36]). The weight of the electric components (battery and motor) is predicted based on the methods previously discussed applying the calculated energy consumption and maximum power on-take.

For the motor design the rotational speed of the driven shaft (LP or HP) is considered assuming no gearbox. The motor operating rotational speed for the CIPH arrangement is higher hence its weight is smaller compared to the MIPH arrangement. The electric power trains predicted weight for the different PMS is presented in Table 5 for the MIPH arrangement and Table 6 for the CIPH arrangement.

For each scenario the aircraft TOW is kept constant, as is the mission range. For accommodating the added weight the payload is reduced accordingly. The weight break – up for the 2500 nm mission and MIPH arrangement is depicted in Figure 19.

Table 5: Electric power train weight for different PMS, MIPH arrangement

Test cases	N_{motor} (rpm)	Weight (kg) 1,000nm	Weight (kg) 2,500nm
TO & PCL (1MW)	5300	185	198
TO & PCL (2MW)	5300	365	377
TO & CL	5300	392	441
Partial Descent	3200	449	490
Descent	3200	598	598
FE DSCNT	3200	1742	1742

Table 6: Electric power train weight for different PMS, CIPH arrangement

Test cases	N_{motor} (rpm)	Weight (kg) 1,000nm	Weight (kg) 2,500nm
TO & PCL (1MW)	16200	121	134
TO & PCL (2MW)	16200	247	259
TO & CL	16200	328	377
Partial Descent	14100	333	382
Descent	14100	482	482
FE DSCNT	14100	1392	1392

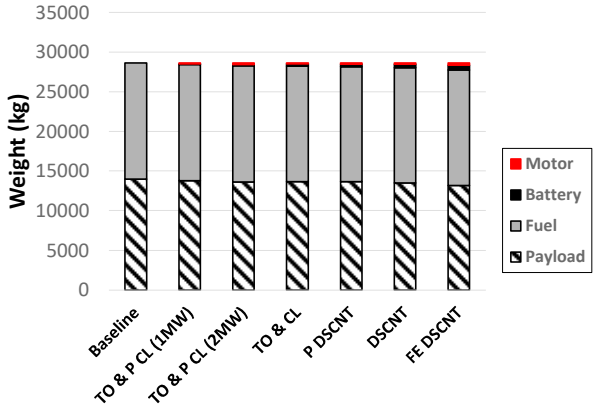

Figure 19: Weight break-up for 2500 nm mission (MIPH arrangement)

Mission Assessment

As seen in Figure 20 and Figure 21 hybridization leads to fuel reduction, as expected. The MIPH arrangement is more efficient than the CIPH in terms of fuel-saving. Moreover, hybrid descent PMS offers higher fuel reduction compared to the T/O & CL PMS. The benefits are rather small to a maximum of 2.5% fuel economy. It is also noted that the potential fuel reduction is greater for the shorter mission, as expected. CO_2 reduction is closely related to fuel consumption, hence MIPH arrangement is more beneficial regarding CO_2 emissions. Based on these results it can be deducted that for achieving a meaningful CO_2 reduction, given the future targets, the duration and degree of hybridisation shall increase significantly.

Driving the LP shaft will reduced fuel flow and compressor discharge temperature and pressure, reducing the emitted NOx, as calculated via the P3T3 method, offering a benefit especially for the high power setting hybridization scenarios, as seen in Figure 22. A reduction of NOx emissions of 3.6% at mission level for the TO & CL PMS is calculated.

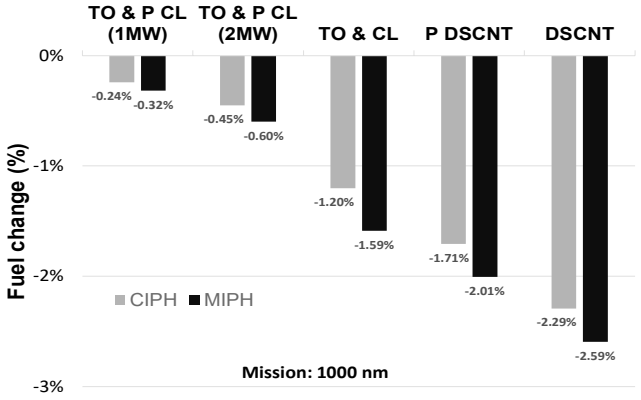

Figure 20: Fuel reduction for different PMS, 1000nm

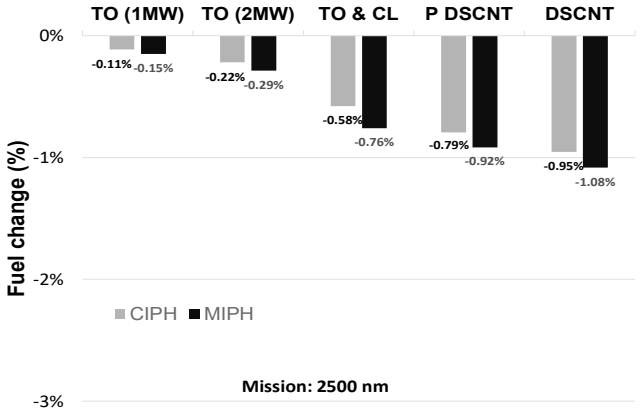

Figure 21: Fuel reduction for different PMS, 2500nm

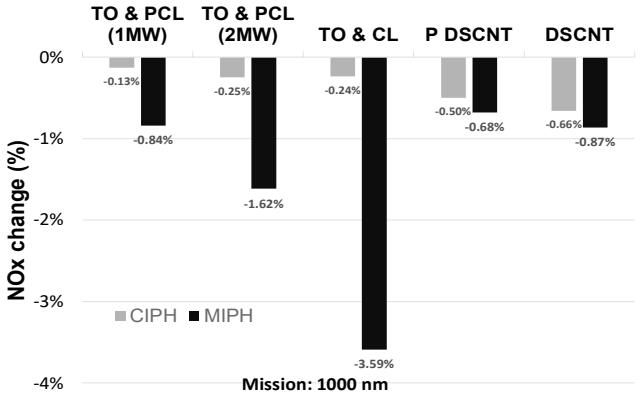

Figure 22: NOx emissions reduction for different PMS, 1000nm

The fuel and emissions reduction comes with a price, since the aircraft payload is reduced. For assessing the hybrid system overall performance, the energy to revenue work (ETRW) ratio is used [37]. Electric energy is added on the nominator for accounting for electrification, as seen in eq. (8).

$$ETRW = \frac{m_f \cdot LHV + E_{electric}}{M_{payload} \cdot g \cdot Range} \quad (8)$$

For examining the potential future benefits of hybridization a second optimistic technology case is considered herein. The key technological parameters that determine the predicted

weight of the electric components are battery specific density and motor active density. The optimistic values of these quantities considered are for the battery 2000Wh/kg (baseline: 1000Wh/kg) and for the motor 4000kg/m^3 (baseline: 8000kg/m^3). It is noted that the results presented are for the 1000nm mission.

As seen in Figure 23 the configurations assessed herein are not expected to outperform the baseline engine in terms of ETRW. It can be highlighted that CIPH arrangement performs better compared to the MIPH when payload is considered. CIPH performance can also be further enhanced if the BOV is optimized to account for the movement of the operating points towards lower pressure ratios. This is expected to be beneficial for the low thrust setting PMS such as the hybrid descent and partial descent. T/O and partial climb PMS may also be of interest since it leads to lower TET, hence positively affecting engine life. In any case potential overall performance benefits, for the aircraft-engine case examined herein may occur only if the electric power train technology evolves significantly.

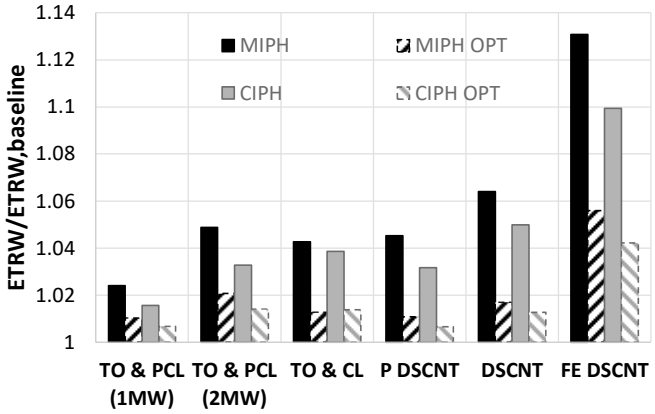

Figure 23: ETRW for HEPS arrangements and 2 technology levels (OPT: 2000Wh/kg 4000kg/m3)

Concerning NOx, the potential benefit in terms of NOx per kg payload is depicted in Figure 24. Hybridizing the T/O and Climb phase is the only case that provides benefits in terms of NOx per kg payload and that occurs only when optimistic future technology is concerned.

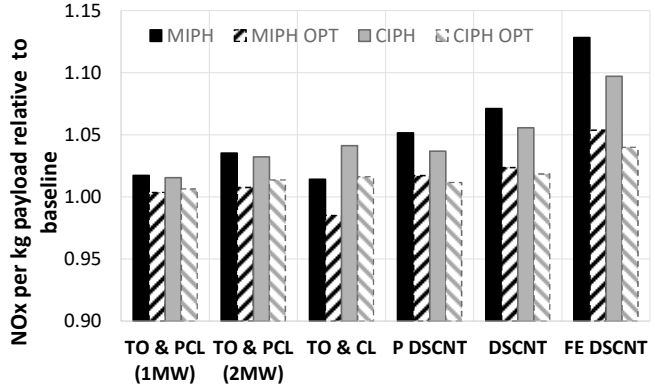

Figure 24: NOx per kg payload for HEPS arrangements and 2 technology levels (OPT: 2000Wh/kg 4000kg/m^3)

CONCLUSIONS

The gas turbine operability and overall performance is assessed for the case of a parallel hybrid electric propulsion system applied to a 150 passenger single-aisle aircraft. Two power on-take arrangements are considered: MIPH and CIPH, boosting the LP shaft and the HP shaft respectively. These arrangements are applied to a year 2000 baseline engine.

The arrangements operability with respect to compressors is evaluated for different DoH and for the 3 representative operating points (T/O, ToC and MCR). The results indicate that operability aspects will impose a limit to hybridization. Components re-matching caused by hybridisation is moving the LPC operation towards surge for the MIPH arrangement and towards choke for the CIPH arrangement. Additionally, the HPC is moving towards high rotational speeds for the case of HP shaft boosting, while for the MIPH case it is the fan that moves towards higher rotational speeds compared to the baseline engine, indicating that mechanical integrity should be considered when hybridization schemes are applied.

The transient simulation indicates that the MIPH arrangement is prone to stalling. The importance of rescheduling the stability BOV is also highlighted, since for the CIPH arrangement BOV closes prematurely, while for the MIPH case it may be needed to increase the bleed off flow during low thrust operation. It is also recognized that there is a potential benefit in rescheduling the BOV for the CIPH arrangement since the LPC operating line is moving away from the surge line, hence bleed off mass flow can be reduced benefiting the engine sfc at low thrust operation.

The two arrangements performance assessment is done for 5 different PMS, for a specific mission and assuming constant aircraft TOW. The results indicate that the MIPH configuration has the potential for higher block fuel economy and NOx emission reduction compared to the CIPH arrangement. These benefits comes at the cost of increased weight, hence the conclusion should be revisited when the ETRW is used as a performance metric. CIPH benefits from lighter electric power train, hence it performs better than the MIPH when available payload is considered. CIPH performance, at low thrust settings, can be further improved if BOV rescheduling is applied, indicating that the arrangement has some advantages which are worth investigating. In any case both arrangements as defined herein cannot outperform the baseline engine for the missions considered (1000nm and 2500nm), even when highly optimistic technology values for the electric power train are applied.

ABBREVIATIONS

BOV	Bleed of Valve
BP	Bypass
CIPH	Cycle-Integrated Parallel Hybrid
CL	Climb
DoH	Degree of Hybridisation
DSCNT	Descent
E	Energy

EPS	Electric Propulsion System
ETRW	Energy to Revenue Work
FE	Fully Electric
FLOPS	Flight Optimisation System
HP	High-pressure
HEPS	Hybrid Electric Propulsion system
ICAO	International Civil Aviation Organisation
LHV	Lower heating value
LP	Low-pressure
m	Mass
m	Mean stator factor
MCR	Cruise
MIPH	Mechanically Integrated Parallel Hybrid
N	Shaft speed in rpm
OPR	Overall Pressure Ratio
P	Power
PMS	Power Management Strategy
sfc	Specific Fuel Consumption
SH	Specific Humidity
T	Temperature
TET	Turbine Entry Temperature
ToC	Top of Climb
T/O	Take-off
V	Volume
W	Mass flow / Weight

SUBSCRIPTS

31	Station 31 (Combustor inlet)
COR	Corrected
F	Fuel
GL	At ground-level

REFERENCES

[1] Airbus, "Global Market Forecast 2019-2038," 2019.

[2] ICAO, "Climate Change," 2020. [Online]. Available: https://www.icao.int/environmental-protection/pages/climate-change.aspx. [Accessed: 23-Jan-2020].

[3] European Commission, "Flightpath 2050: Europe's Vision for Aviation", Report of the High Level Group on Aviation Research, Publications Office of the European Union, Luxembourg, 2011.

[4] Seitz A., Schmitz O., Isikveren A. T., and Hornung M., (2012), "Electrically Powered Propulsion: Comparison and Contrast to Gas Turbines," *Dtsch. Luft- und Raumfahrtkongress 2012*, 281358.

[5] Warwick G., (2020), "What Are The Advantages And Challenges Of Electric-Powered Airliners?," *Aviation week*. [Online].Available: https://aviationweek.com/aerospace/aircraft-propulsion/what-are-advantages-challenges-electric-powered-airliners. [Accessed: 05-Aug-2020]. [Accessed: 05-Aug-2020].

[6] Schneider M., Dickhoff J., Kusterer K., Visser W., Stumpf E., Hofmann J. P., and Bohn D., (2019), "Development of a Gas Turbine Concept for Electric Power," *ASME Turbo Expo 2019*, GT2019-92065.

[7] National Academies of Science, Engineering and Medicine, "Electric Propulsion," in Commercial Aircraft Propulsion and Energy Systems Research: Reducing Global Carbon Emissions, Washington, DC: The National Academies Press, 2016, pp. 51–70.

[8] Seitz A., Nickl M., Stroh A., and Vratny P. C., (2018), "Conceptual study of a mechanically integrated parallel hybrid electric turbofan," *Proc. Inst. Mech. Eng. Part G J. Aerosp. Eng.*, vol. 232, no. 14, pp. 2688–2712.

[9] Masson P. J., Brown G. V., Soban D. S., and Luongo C. A., (2007), "HTS machines as enabling technology for all-electric airborne vehicles," Supercond. Sci. Technol., vol. 20, no. 8, pp. 748–756.

[10] Tomaszewska A., Chu Z., Feng X., O'Kane S., Liu X., Chen J., Ji C., Endler E., Li R., Liu L., Li Y., Zheng S., Vetterlein S., Gao M., Du J., Parkes M., Ouyang M., Marinescu M., Offer G., and Wu B., (2019), "Lithium-ion battery fast charging: A review", eTransportation, vol. 1, p. 100011.

[11] Annapragada S. R., MacDonald M., Sur A., Mahmoudi R., and Lents C., (2018), "Hybrid Electric Aircraft Battery Heat Acquisition System", 2018 AIAA/IEEE Electr. Aircr. Technol. Symp. EATS 2018, 2018-4992, pp. 1–13.

[12] McCluskey F. P., Saadon Y., Yao Z., Shah J., and Kizito J. P., (2018), "Thermal management challenges in turbo-electric and hybrid electric propulsion", 2018 Int. Energy Convers. Eng. Conf., 2018-4695, pp. 1–20.

[13] Simon D. L., Connolly J. W., and Culley D., (2019), "Control Technology Needs for Electrified Aircraft Propulsion Systems," *ASME Turbo Expo 2019*, J. Eng. Gas Turbines Power, vol. 13, GT2019-91413, pp. 1–12.

[14] Sahoo S., Zhao X., Kyprianidis K. G., and Kalfas A., (2019), "Performance Assessment of an Integrated Parallel Hybrid-Electric Propulsion System Aircraft", *ASME Turbo Expo 2019*, GT2019-91459, pp. 1–17.

[15] Wortmann G., Schmitz O., and Hornung M., (2014), "Comparative assessment of transient characteristics of conventional and hybrid gas turbine engine", CEAS Aeronaut. J., vol. 5, no. 2, pp. 209–223.

[16] https://software.nasa.gov/software/LAR-18934-1

[17] Lammen W., and Vankan J., (2020), "Energy Optimization of Single Aisle Aircraft with Hybrid Electric Propulsion", In AIAA Scitech 2020 Forum (p. 0505).

[18] Hoogreef, M., Vos, R., de Vries, R. and Veldhuis, L.L., 2019. Conceptual Assessment of Hybrid Electric Aircraft with Distributed Propulsion and Boosted Turbofans. In AIAA Scitech 2019 Forum (p. 1807).

[19] Roumeliotis I., Nikolaidis T., Pachidis V., Broca O., Unlu D., 2018, "Dynamic Simulation of a Rotorcraft Hybrid Engine

in Amesim", 44th European Rotorcraft Forum, Delft, The Netherlands, 19-20 September, 2018.
[20] Frosina, E., Senatore, A., Palumbo, L., Di Lorenzo, G., Pascarella, C., 2018, "Development of a Lumped Parameter Model for an Aeronautic Hybrid Electric Propulsion System", Aerospace 2018, 5(4), 105.
[21] Hangiu R. P., Filip A. T., Martis C. S., and Biró K. Á., (2012), "System-level Modeling and Simulation of a Permanent Magnet Synchronous Motor for an Integrated Starter Alternator", Journal of Electrical and Electronics Engineering, 5(2):67-70.
[22] Pagonis. M. (2015) 'Electrical Power Aspects of Distributed Propulsion Systems in Turbo-electric Powered Aircraft', PhD thesis, Cranfield University.
[23] MacDonald A. R., (2013) 'Electric Propulsion Modeling for Conceptual Aircraft Design', *51st AIAA Aerospace Sciences Meeting including the New Horizons Forum and Aerospace Exposition*. doi:10.2514/6.2014-0536.
[24] Bradley, K. M., Droney, K. C., (2015) 'Subsonic Ultra Green Aircraft Research: Phase II – Volume II – Hybrid Electric Design Exploration'. Available at: https://ntrs.nasa.gov/archive/nasa/casi.ntrs.nasa.gov/20150017039.pdf
[25] Sahoo, S., Zhao, X., & Kyprianidis, K. (2020). A Review of Concepts, Benefits, and Challenges for Future Electrical Propulsion-Based Aircraft, Aerospace, 7(4), 44.
[26] "Siemens PLM Software Simcenter" https://www.plm.automation.siemens.com/global/en/products/simcenter/
[27] Roumeliotis I, Castro L, Jafari S, Pachidis V, De Riberolles L, Broca O & Unlu D (2021) Integrated systems simulation for assessing fuel thermal management capabilities for hybrid-electric rotorcraft. In: ASME Turbo Expo 2020, London, 21-26 September 2020.
[28] Gaudet S. R., Gauthier J. E. D., (2007), "A simple sub-idle component map extrapolation method," *ASME Turbo Expo 2007*, GT2007-27193.
[29] Martins D. A. R., (2015), "Off-Design Performance Prediction of the CFM56-3 Aircraft Engine", Tecnico Lisboa MSc Thesis.
[30] Lolis, P., (2014), "Development of a Novel Preliminary Aero Engine Weight Estimation Method", PhD Thesis, Propulsion Engineering Centre, Cranfield University.
[31] Ed. Gunston B., 2004, "Jane's Aero-Engines", Issue Fifteen - March 2004, Jane's Information Group Limited.
[32] Pera, R. J., Onat, E., Klees, G. W., Tjonneland, E., (1977), A Method to Estimate Weight and Dimensions of Aircraft Gas Turbine Engines - Final Report Vol. 2 – User's Manual, NASA-CR135170, Seattle, Washington, 1977.
[33] Norman P.D., Lister D.H., Lecht M., Madden P., Park K., Penanhoat O.,Plaisance C., Renger K. Development of the Technical Basis for a New Emissions Parameter Covering the Whole Aircraft Operation: NEPAIR, Final Technical Report NEPAIR/WP4/WPR/01; 2003.
[34] ICAO, "ICAO Aircraft Engine Emissions Databank," 2019. [Online]. Available: https://www.easa.europa.eu/domains/environment/icao-aircraft-engine-emissions-databank. [Accessed: 25-Apr-2020].
[35] Lents, C.E.; Hardin, L.W.; Rheaume, J.; Kohlman, L. Parallel Hybrid Gas-Electric Geared Turbofan Engine Conceptual Design and Benefits Analysis. In Proceedings of the 52nd AIAA/SAE/ASEE Joint Propulsion Conference, Washington, DC, USA, 13–17 June 2016; p. 4610.
[36] Masson, P.J., Pienkos, J.E. and Luongo, C.A., 2007. Scaling up of HTS motor based on trapped flux and flux concentration for large aircraft propulsion. IEEE transactions on applied superconductivity, 17(2), pp.1579-1582.
[37] Agarwal, R. and Zhang, Z., "Optimization of ETRW (Energy Liberated During a Flight/Revenue Work Done) of an Airplane for Minimizing its Environmental Impact," SAE Technical Paper 2011-01-2524, 2011.